Journal Article

Formation of chitosan nanoparticles to encapsulate krill oil (Euphausia superba) for application as a dietary supplement

Haidera, J., Majeeda, H., Williams, P.A., Safdara, W. and Zhonga, F.

Formation of chitosan nanoparticles to encapsulate krill oil (*Euphausia superba*) for application as a dietary supplement

Junaid Haider[a], Hamid Majeed[a], P.A. Williams[b], Waseem Safdar[a], Fang Zhong[a]*

[a]State Key Laboratory of Food Science and Technology, School of Food Science and Technology, Jiangnan University, Wuxi 214122, Jiangsu, People's Republic of China.

[b]Center for Water Soluble Polymers, Glyndwr University, Wrexham, Wales LL11 2AW, UK

Corresponding author:
Fang Zhong
[a]State Key Laboratory of Food Science and Technology,
School of Food Science and Technology,
Jiangnan University, Wuxi 214122,
Jiangsu, People's Republic of China.
Tel., +8613812536912. Fax: +8651085329060.
E-mail address: fzhong@jiangnan.edu.cn

Formation of chitosan nanoparticles to encapsulate krill oil (*Euphausia superba*) for application as a dietary supplement

Junaid Haider, Hamid Majeed, P.A. Williams, Waseem Safdar, Fang Zhong

Abstract:

Encapsulation of krill oil (KO), a rich source of eicosapentanoic (EPA) and docosahexanoic acid (DHA) was carried out in chitosan-TPP (tripolyphosphate) nanoparticles using a newly developed two-step process (i.e, formation of emulsion and later electrostatic interaction of chitosan with TPP). The encapsulation of KO in chitosan nanoparticles (CSNPs) was confirmed by using Fourier transform infrared spectroscopy (FTIR), X-ray diffraction (XRD) and Thermo gravimetric analysis (TGA) techniques. Loading capacity (LC) and encapsulation efficiency (EE) of the obtained particles were about 9 – 25 and 33 – 59 % respectively, when the initial KO content was in the ratio of 0.25 – 1.25 g/g of Chitosan. Bulk KO showed less protection to oxidation and showed more formation of hydroperoxides during first week as noted by FTIR. However, KO loaded CSNPs showed better prevention of KO towards oxidation with less hydroperoxide formation even after two weeks of storage at elevated temperature (45 ^{o}C). The obtained KO-loaded CSNPs were irregular in shape with an average particle diameter of < 130 nm as observed by SEM. The results obtained confirmed the suitability of the emulsion and later electrostatic interaction of CS with TPP for the formation of KO loaded CSNPs with greater EE & LC, which will enhance their usage in the Food and Pharmaceutical industries.

Key Words: Krill Oil, Fourier transform infrared spectroscopy (FTIR), X-ray diffraction (XRD), Thermo gravimetric analysis (TGA), Oxidative stability

1. Introduction

Antarctic Krill (*Euphausia superba*) has recently emerged as a potential and rich alternative source of long chain omega-3 polyunsaturated fatty acids (LC ω-3 PUFAs) besides the algal and fish oils to be substituted as a dietary supplements. Krill oil (KO) contains long chain omega-3 polyunsaturated fatty acids (LC ω-3 PUFAs), namely eicosapentaenoic acid (EPA, 20:5) and docosahexaenoic acid (DHA, 22:6) (Grandois, Marchioni, Minjie Zhao, Ennahar, & Bindler, 2009). The fatty acids in fish oil are stored as triglyceride, whereas in KO approximately 30 – 65

% of the fatty acids are predominantly incorporated into phospholipids (Schuchardt et al., 2011; Tou, Jaczynski, & Chen, 2008). The particular and unique amphiphilic structural arrangement of phospholipids provides KO with a much better bioavailability (Schuchardt et al., 2011). Moreover, KO contains naturally occurring powerful antioxidants mainly astaxanthin (Deutsch, 2007; Tou et al., 2008). Various researchers recommend use of KO to prevent chronic disorders like cardiovascular diseases, endocannabinoide, poor infant development, non-alcoholic fatty liver disease, premenstrual syndrome, inflammation and certain cancers. This preventive effect was credited to the synergistic action between KO constituents LC ω-3 PUFAs, phospholipids and astaxanthin (Deutsch, 2007; Sampalis et al., 2003; Tur, Bibiloni, Sureda, & Pons, 2012). However, its limited solubility in water and rapid instability to oxidation had made it difficult to achieve these benefits (Bustos, Romo, Yáñez, Díaz, & Romo, 2003).

To avoid limited solubility (Dispersibility in aqueous media), and the oxidative instability of lipophilic compounds like KO, various researchers encapsulate them in protein and carbohydrate based matrices (Ilyasoglu & El, 2014; Zimet & Livney, 2009). In addition to the above mentioned benefits, nanoencapsulation of lipophilic compounds also increased their bioavailability (Fathi, Mozafari, & Mohebbi, 2012). However, protein and polysaccharides that have been used widely to encapsulate lipophilic compounds play a key role in attaining the benefits (Chen & Subirade, 2005; Wang et al., 2006). For example, Majeed et al, prepared clove oil loaded nanoemulsions using modified starch and Tween 80 based surfactants and attained controlled release of oil from starch based nanoemulsions. However, Tween 80 adsorbed onto the droplet and failed to provide the desired release of oil (Majeed et al., 2016).

Chitosan (CS), a cationic polysaccharide that has been used widely for encapsulation and delivery of lipophilic compounds due to its biodegradability (enzymatically degraded (Lysozyme) into fragments suitable for renal clearance), biocompatibility, non-antigenicity and low toxicity (Malafaya, Silva, & Reis, 2007). Recently, researchers used a two-step emulsion and ionic-gelation method to produce CS-TPP nanoparticles due to its simplicity and non-toxicity for targeted delivery of bioactives (Malafaya et al., 2007; Yang et al., 2011). In the two step, emulsion ionic-gelation procedure the latter involves electrostatic interaction between cationic groups of CS and anionic groups of TPP (Calvo, Remuñán-López, Vila-Jato, & Alonso, 1997; Kawashima et al., 1985; Yang et al., 2011). The electrostatic interaction between cationic groups of CS and anionic groups of TPP occurred by inter and intramolecular bonds (Calvo et al., 1997; Kawashima et al., 1985; Yang et al., 2011). Ionic-gelation based CSNPs have been used widely for the encapsulation, and targeted delivery of proteins (Kawashima et al., 1985; Xu & Du, 2003), essential oils (Hosseini, Zandi, Rezaei, & Farahmandghavi, 2013; Keawchaoon & Yoksan, 2011), drugs (Wang et al., 2006; Wu, Yang, Wang, Hu, & Fu, 2005), vitamins and nutrients (Chen & Subirade, 2005; Yoksan, Jirawutthiwongchai, & Arpo, 2010). Keawchaoon and Yoksan revealed successful encapsulation of carvacrol in CS-TPP particles with extended shelf life and well retained functional properties (Keawchaoon & Yoksan, 2011). Similarly, Hosseini et al, prepared oregano oil loaded CS-TPP nanoparticles by an additional step of oil-in-water emulsification prior to solidification of these droplets by CS & TPP (Hosseini et al., 2013). They confirmed regularly distributed, spherical shaped particles having size 40 – 80 nm with slow release characteristics. They reported more than 80 % release of oregano oil that was attributed to greater surface volume ratio due to smaller particle size. On the other hand, nano-capsules due to larger size reduced the surface volume ratio and ultimately influence the access of digestive enzyme, dispersibility of their products and finally influenced the efficacy of delivery system (Kim, Diab, Joubert, Canilho, & Pasc, 2016; Majeed et al., 2016). However,

loading of KO having a distinctive chemical structure of LC ω-3 PUFAs into CSNPs at a nano-level size has not been elucidated. Therefore, the current study focuses on the fabrication, characterization and oxidative stability of KO loaded in CSNPs by two step process: oil-in-water emulsification, and ionic gelation (CS & TPP).

2 Materials and methods

2.1 Materials

Antarctic krill oil contained ~40 % total phospholipid, ~28 – 30 % total omega-3 fatty acids and ≤ 200 mg/kg astaxanthin as stated by the manufacturer (Hutai Biopharm Inc. (Sichuan, China). Partially deacetylated chitosan (CS; degree of deacetylation of 91.5 %), with average molecular weight of 100 kDa derived from crab shells was obtained from Golden-Shell Biochemical Co., Ltd. (Hangzhou, China). CS is a weak polyelectrolyte with a pKa value around 6.5, which is positively charged in acidic conditions (Fan, Yan, Xu, & Ni, 2012). Tween 80, glacial acetic acid, Sodium tripolyphosphate (TPP) and all other chemicals used were of analytical grade, purchased from Sinopharm Chemical Reagent Co., Ltd., China. Double distilled water was used throughout this study.

2.2 Preparation of KO-loaded CSNPs

KO-loaded CSNPs were prepared using a modified version of the method described by (Calvo et al., 1997) and (Hosseini et al., 2013). A schematic illustration representing the CSNPs preparation procedure is shown in **Fig. 1**. Briefly, CS solution 1.5 % (w/v) was prepared by agitating CS in an aqueous acetic acid solution 1 % (v/v) at ambient temperature (25 – 28 ^{o}C) for 24 h. The CS solution was centrifuged at 8000 rpm for 20 min, the supernatant was filtered through a 0.8 µm pore size syringe filter. Tween 80 (0.5g, hydrophilic-lipophilic balance = 15) was added as a surfactant to the CS solution (40 mL) and the mixture was stirred at 45 ^{o}C for 2 h to obtain a homogeneous solution. KO was gradually dropped into the aqueous CS solution (40 mL) and the system was homogenized using an Ultra-Turrax (T25, Ika-Werke, Staufen, Germany) at a speed of 13,000 rpm for 1 min and 16,500 for 2 min. The solution was positioned in an ice-bath to prevent heating. The content of KO was varied (0, 0.15, 0.30, 0.45, 0.60 and 0.75 g) to obtain different weight ratios of CS to KO (1:0, 1:0.25, 1:0.50, 1:0.75, 1:1.00 and 1:1.25 respectively). Subsequently, TPP solution (0.5 % v/v, 40mL) was then added drop wise into the o/w emulsion under continuous stirring and was agitated for 40 min. The particles formed were collected by centrifugation at 10,000 × g for 30 min at 20 ^{o}C and washed several times with water to remove or wash off excessive KO. Eventually, the wet particles were dispersed in 25 mL water by ultrasonication to produce a homogeneous suspension. Ultrasonication was performed using a (Jy98-IIIDN, 20 kHz, Ningbi Scientz Biotechnology Co., Ltd., Ningbo, China) sonicator for 2 min in an ice bath. The suspensions were immediately freeze-dried at – 35 ^{o}C for 72 h and were stored in dry conditions at 25 ^{o}C.

2.3 Characterization of KO-loaded CSNPs

2.3.1 Z-average diameter and ζ-potential measurements

The z-average diameter and the uniformity of particles in dispersion (particle size distribution) that is being measured as polydispersity index (PDI) for KO-loaded CSNPs were investigated by dynamic light scattering (DLS) using the Zetasizer Nano ZS® (Malvern

Instruments, Worcestershire, U.K.). To avoid multiple scattering effects, the nanoparticles were diluted 100-fold with purified water, placed in a cuvette and agitated well prior to measurements. Refractive indices of 1.45 for KO and 1.330 for water were used. ζ-potential was determined by Laser Doppler Velocimetry using the Zetasizer Nano ZS® at a scattering angle of 173° at 25 °C. The diluted nanoparticles were placed in a folded capillary electrophoresis cell with count rate between 100 and 300 Kcps as described by Zainol et al. (Zainol et al., 2012). All the tests were performed in triplicate.

2.3.2 Morphology of KO-loaded CSNPs

The morphological characterization of the nanoparticles was done using SEM (Hitachi S-4800, Japan) at an accelerating voltage 2 kV. The powders were sprinkled onto double-backed cellophane tape attached to an aluminium stub before coating with gold-palladium in an argon atmosphere.

2.3.3 Characterization using FTIR, TGA and XRD

The infrared spectra of all samples were obtained using a Thermo Fisher Scientific Inc., Nicolet iS10, FTIR spectrometer with KBr accessory. This instrument was operated with Nicolet OMNIC software (Version 8.2). For KO spectral acquisition, the liquid sample (≈ 2 μL) was deposited on a KBr disk. The spectra were obtained using 16 scans at a resolution of 4 cm^{-1} over the frequency range of 4000 – 400 cm^{-1}. Before running each sample a background spectrum was obtained in air.

Contact angle was used to determine the interaction between KO and nanoparticles with sessile drop method. Briefly, KO (3 μL) was carefully dropped with a dosing rate of 0.5 μL/s onto the slides (20 mm × 50 mm × 1 mm) using 2 mL micrometer syringe (KDL Corp., Shanghai, China). The measurements were carried out in open air with relative humidity (30%) and at a room temperature of 25 °C. Both left and right contact angles expressed in degrees were automatically calculated from the digitalized image software belonging to the equipment (DataPhysics Instruments GmbH, OCA15EC, Germany). Measurements were taken in triplicate of each sample.

TGA was performed using a TGA/DSC 1 STARe (Mettler-Toledo, Switzerland) 25 – 600 ^{o}C with a heating rate of 10 ^{o}C/min under nitrogen atmosphere. Each freeze-dried sample 6 – 10 mg was placed in the TGA furnace. The derivative thermogravimetric curves (DTG) and the first derivative of TG curves were calculated.

XRD patterns of packing materials were assessed by X-ray diffraction using a (Bruker AXS D8, Germany) diffractometer. The operation conditions were 40 kV and 40 mA with Cu Kα radiaton (λ = 1.5406 Å). Samples were scanned in the 2θ range of 5^{o} – 50^{o} at a speed of 0.03^{o} per second.

2.4 Determination of loading capacity (LC) and encapsulation efficiency (EE)

The content of KO-loaded CSNPs was determined by TGA/DTG. Freeze dried CSNPs and KO-loaded CSNPs were placed in TGA furnace at 25 – 600 ^{o}C with a heating rate of 10 ^{o}C/min under nitrogen atmosphere and the weight loss percentage, obtained from TGA thermograms was used to determine the content of KO-loaded CSNPs. The loading capacity of KO (g/100g of sample) and encapsulation efficiency of KO (g/100g of sample) were thus calculated from **eqs. (1)** and **(2)** respectively.(Yoksan et al., 2010)

$$\text{LC (\%)} = \frac{\text{wight of loaded KO}}{\text{Weight of sample}} \times 100 \qquad (1)$$

$$\text{EE (\%)} = \frac{\text{wight of loaded KO}}{\text{Weight of initial KO}} \times 100 \qquad (2)$$

2.5 Storage conditions

For the lipid oxidation experiments, five grams of bulk oil and freeze-dried KO-loaded CSNPs were placed in 20 ml loosely capped amber glass bottles. Samples were stored at 45 ^{o}C for 4 weeks. The extent of lipid oxidation was investigated in terms of lipid hydroperoxide. All the experiments were carried out in duplicate.

2.5.1 Determination of lipid oxidation

In this study, lipid hydroperoxides, the primary oxidation products was monitored by FTIR (Guillén & Cabo, 1999, 2002). Each band frequency was obtained automatically from the instrument software command "find peaks" with an adequate threshold value near 85 %. The functional group vibration mode of each band was made by comparison with software spectral library as well as with literature data and similar experimental conditions of FTIR was applied for sample acquisition as utilised to confirm the loading of KO in CSNPs (See section 2.3.3).

3 Results and discussion

3.1 Shape, size and surface charge of KO-loaded CSNPs

KO-loaded CSNPs were prepared through the formation of oil droplets (including KO) and droplet solidification. The KO droplet formation in CS solution was achieved using the O/W emulsion technique. The solidification of each droplet was extended by ionic cross-linking of ammonium groups of CS molecules surrounding the KO droplet and phosphate groups of TPP.

The surface morphology of CSNPs and KO-loaded CSNPs were observed by SEM. **Fig. 2 (a, b)** shows the CSNPs size varied between 100 – 300 nm that correlates with the findings of Yoskan (Yoksan et al., 2010). For KO-loaded CSNPs, the aggregations were also seemed that might be due to remaining KO around the particles with an average range of 80 – 130 nm **(Fig. 2-c, d)**.

The z-average diameter and PDI of CSNPs and KO-loaded CSNPs were examined by dynamic light scattering (DLS). **Fig. 3** shows that the z-average diameter and PDI of CS particles were about ~252 nm and 0.199, respectively. The z-average diameter of KO-loaded CSNPs were in the range of 229.5 – 182.4 nm. With increasing ratio of KO, the z-average diameter decreased **(Table 1)**. The possible reason behind this reduction in particle size might be the coemulsifying properties of the oil constituents in the presence of surfactant that reduces the interfacial tension as various researchers reported this phenomenon for essential oil loaded nanoemulsions (Majeed, Antoniou, & Fang, 2014; Terjung, Löffler, Gibis, Hinrichs, & Weiss, 2012). However, the agglomeration and/or swelling of KO-loaded CSNPs in water were lower than those of CS particles. The obvious difference in the agglomeration of two nanoparticulate systems is the formation mechanism. The CS particles are formed by the electrostatic interaction of CS and TPP and their size will depend on how the molecules were mixed together. On the other hand, KO-loaded CSNPs are formed by the adsorption of CS onto the KO droplets. The lower agglomeration in KO-loaded CSNPs might be due to hydrophobic KO molecules that forced it to

entrap inside (Keawchaoon & Yoksan, 2011; Yoksan et al., 2010). The interesting fact about KO is that it possesses a large proportion of marine phospholipids (about 40 %) bonding with LC ω-3 PUFAs like EPA and DHA (Zhu, Zhuang, Luan, Sun, & Cao, 2015). Similarly, Shen and Lu et al. reported small z-average diameter of nanoparticles that can be credited to phospholipids in KO, having substantial inherent emulsifying power (Lu, Nielsen, Baron, Jensen, & Jacobsen, 2012; Shen, Bhail, Sanguansri, & Augustin, 2014).

In addition, ζ-potential of CSNPs gave a positive charge of + 37.7 mV as shown in **Fig. 3**. The positive surface charge arises due to ammonium groups of CS. With loading of KO, the ζ-potential was decreased to + 26.6 mV. This reflects the CSNPs surface with increasing KO content. The reduction in ζ-potential value was related to the number of TPP to CS charge groups as evident by the findings of (Antoniou et al., 2015). However, this reduction might be due to shielding effect of protonated $–NH_2$ group by KO on CSNPs. Several studies have reported that ζ-potential values of CSNPs was reduced when drugs, i.e., ascorbic acid (Jang & Lee, 2008) and eugenol were (Woranuch & Yoksan, 2013) incorporated. This demonstrated that ζ-potential value influenced reciprocally with increased drug content.

3.2 Characterization of KO-loaded CSNPs

CSNPs loaded with KO were characterized by Fourier Transform Infrared spectroscopy (FTIR). The results confirmed the presence of KO with characteristic peaks at 3416 cm^{-1} (OH), 3012 cm^{-1} (=C–H stretching), 3000 – 2800 cm^{-1} (C–H stretching), 1740 cm^{-1} (C=O stretching band), 1465 cm^{-1} ($–CH_2–$ bending), 1379 cm^{-1} ($–CH_3$ bending), 1091 cm^{-1} (CO stretching), 971 cm^{-1} (C=C stretching band) as shown in **Fig. 4a**.

However, CSNPs showed characteristics bands at 3450 cm^{-1} (OH), 2927 cm^{-1} (CH stretching), 1640 cm^{-1} (amide I), 1543 cm^{-1} (amide II), 1155 cm^{-1} (P=O), 1097 cm^{-1} (COC) and 891 cm^{-1} (pyranose ring) that suggests the complex formation between CS and TPP as a result of electrostatic interaction **Fig. 4b** (Bhumkar & Pokharkar, 2006; Xu & Du, 2003). Moreover, FTIR confirmed the incorporation of KO in CSNPS **(Fig. 4 c-g)** by comparing with characteristic peaks in the KO spectra. The occurrence of characteristic peak at same wave number in KO loaded CSNPs indicating no interaction with chitosan. Similarly, non-interaction behaviour of chitosan (hydrophilic) with oregano oil (hydrophobic) has earlier been reported by Hosseini et al when incorporated in CS-TTP nanoparticles (Hosseini et al., 2013). Further, this interaction was investigated using contact angle measurement and also showed no interaction between KO and CSNPs as shown in Figure **Fig. 5.** The contact angle of KO and CSNPs with air was 38.35 and 25.84, respectively as shown in **Fig. 5a & b**. However, in case of increasing ratios of KO in loaded CSNPs the contact angle increased (26.28 – 36.46) that suggests increased hydrophobicity of KO **(Fig. 5 c–g)**. On the other hand, with maximum KO loaded CSNPs (1:1 & 1: 1.25) showed significant increase in contact angle (10 degree rise). Whereas, at lower ratios (1: 0.25 – 1: 0.75) of KO loaded CSNPs the contact angle was quite same (26.28 & 31.21) as appeared in KO with unloaded CSNPs (Fig. c,d). The possible reason behind this increase in contact angle at highest CS:KO mass ratios is the exposure of excessive oil to standard drop of KO (3 ul) used during this experimental procedure that resulted in increased hydrophobicity. These findings revealed that CS and CSNPs showed no interaction with KO. Contact angle measurement has already been used by variety of researchers to explain the interaction behaviour of hydrophobic and hydrophilic compounds (Liu et al., 2016; Shamsijazeyi et al., 2014).

On the other hand, the increase in CH stretching peak intensity at 2869 – 2974 cm^{-1} reflects the location of KO in the CS matrix. These results were further strengthened as the increase in CH stretching peak intensity was observed with increasing KO content. Therefore, we can

consider CH stretching as a strong indicator of KO encapsulation in any matrix (Vongsvivut et al., 2012; Zhao, Wei, Liu, & Liu, 2014). Thus, emulsion and later electrostatic interaction of CS with TPP, a two-step process successfully encapsulated KO in CSNPs. (Section 3.3)

TGA has been used widely by a variety of researchers to confirm the weight change of material that is monitored as a function of temperature to evaluate its thermal stability (Yoksan et al., 2010). In our case, the degree of weight loss for CS alone and KO loaded CSNPs decreased with increasing temperature from 25 to 600 ^{o}C as shown in **Fig. 6A**. KO degradation showed one level of weight loss **Fig. 6A (a)**. Whereas, CS and KO loaded CSNPs showed two **(Fig. 6A-b)** and three levels of weight loss **Fig. 6A (c-g)**. Nam et al. reported the first and second level of weight loss for CS nanofibers that showed temperature ranges from 56 to 115 ^{o}C and 182 – 310 ^{o}C, which corresponded to evaporation of moisture and decomposition of polymer, respectively (Nam, Park, Ihm, & Hudson, 2010). The rate of maximum weight loss corresponding to temperature was determined as the decomposition temperature (T_d), which is clearly observed as a peak in the derivative thermogravimetry (DTG) thermogram, plotted in **Fig. 6B**. From the DTG thermogram, CSNPs exhibited one level T_d at 247 ^{o}C **(Fig. 6B-b)**. By comparison between CS and KO-loaded CSNPs manifested new T_d range 327 – 331 ^{o}C **(Fig. 6B (c-g)**, which corresponded to the T_d of KO **(Fig. 6B-a)**. The results confirmed the successful loading of KO into CSNPs. Similarly, Yoksan et al. reported increased thermal stability of successfully encapsulated ascorbyl palmitate in CSNPs (Yoksan et al., 2010). The weight loss percentage at this temperature range was thus used to compute the quantity of loaded KO (section 3.3)

XRD patterns of CS powder, CSNPs, and KO-loaded CSNPs are presented in **Fig. 7**. Generally, CS exhibits two peaks at 2θ of 10^{o} and 20^{o} **(Fig. 7a)**, showing high degree of crystallinity. After electrostatic interaction with TPP, peak broadening and peak shifts were observed with reduction of peak intensity **(Fig. 7b)**. In addition, a new peak is found in the diffractogram of CSNPs at 2θ of 23^{o}. These distinct differences reflect the modification in the arrangement of molecules in the crystal lattice stimulated by ionic interaction (Bhumkar & Pokharkar, 2006; Yoksan et al., 2010). As compared with CSNPs, in the diffraction spectrum of KO-loaded CSNPs the characteristic peaks at 2θ of 18^{o} confirmed the presence of KO within CSNPs. Thus, XRD analysis revealed the successful encapsulation of KO in CSNPs as it clearly showed change in the CS-TPP packing structure. So, on behalf of FTIR, TGA, and XRD we can conclude that two steps, emulsion and electrostatic interaction between CS and TPP is suitable for the encapsulation of KO in CSNPs.

3.3 Encapsulation efficiency and loading capacity

The TGA/DTG technique was applied for quantitative analysis of CSNPs in terms of weight loss at temperature ranging from 290 – 380 ^{o}C, corresponding to T_d of KO. The percentage of LC and EE of KO-loaded CSNPs were then calculated using **Eqs. (1)** and **(2)**, respectively, and are tabulated in **Table 1**. From TGA results, the percentage of LC was in the range of 8.8 to 24.7 % at 25 to 125 % (w/w) ratio of KO to CS **(Table 1)**. LC percentage was dependent on initial KO content that was in agreement to the findings of other researchers who reported carvacrol or BSA loading in CSNPs was initial concentration dependent (Keawchaoon & Yoksan, 2011; Xu & Du, 2003). EE of KO ranged from 33.3 to 58.9 %. Maximum EE value (58.9 %) was achieved at 1:0.25 (w/w) CS to KO ratio. However, with the increase of KO ratio, EE started to decrease as shown in **Table 1**. This might be due to saturation of CSNPs with KO (Hosseini et al., 2013; Yoksan et al., 2010), as it possesses a large proportion of marine phospholipids bonded with LC-PUFA and astaxanthin. No doubt, large proportion of phospholipids (about 50 %) in KO bounds with DHA, EPA and astaxanthin, which enhanced the solubility of these constituents in lipid

phase that consequently reduced its diffusion outside the nanoparticles (Zhu et al., 2015). The reduction in EE with increasing KO content suggests its loading in CSNPs is limited.

In addition to EE, LC was determined by FTIR using the CH stretching peak to determine the content of KO in CSNPs. The CH stretching peak at 2925 cm^{-1} and the pyranose peak at 891 cm^{-1} were used as representative peaks of KO and CS, respectively. The CH stretching to pyranose peak (I_{2925}/I_{891}) is shown in **Table 1**. CSNPs showed an I_{2925}/I_{891} value of 0.91 and for KO-loaded CSNPs, the value of I_{2925}/I_{891} was greater than 0.91 suggesting successful loading of KO in the nanoparticles. KO-loaded CSNPs with initial KO content (0.25 – 1.25 g/g) of CS showed I_{2925}/I_{891} values in the range of 1.14 – 1.81. The value of I_{2925}/I_{891} increased with increasing initial KO content. However, KO-loaded CSNPs with an initial KO content of 1 g/g of CS provided the maximum value of I_{2925}/I_{891} as shown in **Table 1**. These results confirmed the findings of TGA and we can conclude that the optimal weight ratio of CS to KO was 1:1.

3.4 Oxidative stability

The oxidative stability of bulk KO and KO containing CSNPs was evaluated using FTIR spectra that were determined after exposure with elevated oxidative stress (45 ^{o}C). FTIR spectroscopy has been used earlier to identify change in the functional groups of the sample that undergoes lipid oxidation (Voort, Ismail, Sedman, & Emo, 1994). **Fig. 8** illustrates obvious spectral changes in krill oil spectra as oxidation proceeds. However, peak shift in the ROOH region from ~3416 cm^{-1} to ~3377 suggests the formation of hydroperoxides (**Fig. 8-A).** Whereas change in CO (initial absorption at ~1091 & ~1077 cm^{-1} and gradual shifting to ~1093 & ~1065 cm^{-1} respectively) and *trans* region confirmed the formation of conjugated trans species (~971 cm-1) along with isolated trans absorptions (~969 cm^{-1}) as presented in (**Fig. 8-B).** In the case of KO containing CSNPS the ROOH peak shift varied with CS-KO weight ratios. For 1:1, it was moved to ~3431 to ~3404 cm^{-1} and ~3424 to ~3389 cm^{-1} at 1:1.25 ratio (**Fig. 8-C**)**.** On the other hand, the triglyceride ester group peak shifts showed less dependency to CS-KO weight ratios and it was from ~1741 to ~1739 cm^{-1} at 1:1 & 1:1.25 CS-KO weight ratios as shown in **Fig. 8-D**.

The occurrence of a larger shift ~39 cm^{-1} (~3416 – ~3377 cm^{-1}) in the ROOH band under oxidative stress as shown in **Fig. 8** has already been confirmed (Voort et al., 1994). Moreover, there was a shift back to higher wavenumbers (~3425) that might be due to breakdown of hydroperoxides to alcohols as evident by the findings of Gullién & Cabo and Voort et al. (Guillén & Cabo, 1999; Voort et al., 1994). In contrast a band shift of ~12 cm^{-1} of CO groups in the esters and only a slight (1 – 2 cm^{-1}) shift in *cis*, conjugated *trans*, and isolated *trans* bands occurred. The KO showed an obvious decrease in the ROOH band and triglyceride ester groups during the first week of storage. KO-loaded CSNPs showed a modest decrease in band shifts even after two weeks of storage that suggests more oxidation prevention of KO in CSNPS.

The oxidation prevention of KO in KO-loaded CSNPs in terms of little change in band shift of ROOH and triglyceride ester groups under oxidative stress showed less availability of hydroperoxides to convert them back to aldehydes and ketones (Guillén & Cabo, 2002). Similary Gullién and Cabo also reported a shift of the ROOH band towards lower wavenumbers as oils underwent oxidation, but to a somewhat lesser extent (Guillén & Cabo, 1999). Thus, it may be postulated that the ROOH band shift is due to extensive intermolecular hydrogen bonding of hydroperoxides (Russin, van de Voort, & Sedman, 2003).

4 Conclusion

The KO loaded CSNPs were prepared by a two-step, emulsion and later electrostatic interaction of CS with TPP showed average diameter of 80 – 130 nm as observed by SEM. The

loading capacity (LC) and encapsulation efficiency (EE) of KO in nanoparticles was about 8.8 to 24.7 % and 33.3 to 58.9 %, respectively, when the ratio of KO to CS was 25 – 125 %. Moreover, the loading of KO into CSNPs was confirmed by the increment of CH stretching peak intensity at 2869 – 2974 cm^{-1} (FTIR technique), a degradation temperature of 327 – 331 ^{o}C (TGA/DTG techniques), and the characteristic peaks at 2θ of 18^{o} (XRD technique). Further, CSNPS were successful in preventing the oxidation of KO. The results confirmed the suitability of the emulsion and electrostatic interaction based method for the formation of KO loaded CSNPs with greater EE & LC that will enhance their usage in food and pharmaceutical industry. But, prior to their industrial usage further research is needed on the sensory perception, bioavailability and protection of encapsulate deterioration during product shelf life.

Acknowledgement

This work was financially supported by National 125 program 2011BAD23B02; NSFC 31571891 and 31401533; JUSRP 51507 and 11422; 111Project B07029 and PCSIRT0627.

References

Antoniou, J., Liu, F., Majeed, H., Qi, J., Yokoyama, W., & Zhong, F. (2015). Physicochemical and morphological properties of size-controlled chitosan–tripolyphosphate nanoparticles. *Colloids and Surfaces A: Physicochemical and Engineering Aspects*, *465*, 137–146.

Bhumkar, D. R., & Pokharkar, V. B. (2006). Studies on effect of pH on cross-linking of chitosan with sodium tripolyphosphate: a technical note. *AAPS PharmSciTech*, *7*(2), E50.

Bustos, R., Romo, L., Yanez, K., Diaz, G., & Romo, C. (2003). Oxidative stability of carotenoid pigments and polyunsaturated fatty acids in microparticulate diets containing krill oil for nutrition of marine fish larvae. *Journal of Food Engineering*, *56*(2-3), 289–293.

Calvo, P., Remunan-Lopez, C., Vila-Jato, J. L., & Alonso, M. J. (1997). Novel hydrophilic chitosan-polyethylene oxide nanoparticles as protein carriers. *Journal of Applied polymer science*, *63*(1), 125–132.

Chen, L., & Subirade, M. (2005). Chitosan/β-lactoglobulin core-shell nanoparticles as nutraceutical carriers. *Biomaterials*, *26*(30), 6041–6053.

Deutsch, L. (2007). Evaluation of the effect of Neptune Krill Oil on chronic inflammation and arthritic symptoms. *Journal of the American College of Nutrition*, *26*(1), 39–48.

Fan, W., Yan, W., Xu, Z., & Ni, H. (2012). Formation mechanism of monodisperse, low molecular weight chitosan nanoparticles by ionic gelation technique. *Colloids and Surfaces B: Biointerfaces*, *90*(1), 21–27.

Fathi, M., Mozafari, M. R., & Mohebbi, M. (2012). Nanoencapsulation of food ingredients using lipid based delivery systems. *Trends in Food Science and Technology*, *23*(1), 13–27.

Grandois, J. L. E., Marchioni, E., Minjie Zhao, F. G., Ennahar, S., & Bindler, F. (2009). investigation of natural phosphatidylcholine sources: separation and identification by liquid chromatography-electrospray lonization-tandem mass spectrometry (lc-esi-ms2) of molecular species. *Journal of Agricultural and Food Chemistry*, *57*(14), 6014–6020.

Guillén, M. D., & Cabo, N. (1999). Usefulness of the Frequency Data of the Fourier Transform Infrared Spectra To Evaluate the Degree of Oxidation of Edible Oils. *Journal of Agricultural and Food Chemistry*, *47*(2), 709–719.

Guillén, M. D., & Cabo, N. (2002). Fourier transform infrared spectra data versus peroxide and anisidine values to determine oxidative stability of edible oils. *Food Chemistry*, *77*(4), 503–510.

Hosseini, S. F., Zandi, M., Rezaei, M., & Farahmandghavi, F. (2013). Two-step method for encapsulation of oregano essential oil in chitosan nanoparticles: Preparation, characterization and in vitro release study. *Carbohydrate Polymers*, *95*(1), 50–56.

Ilyasoglu, H., & El, S. N. (2014). Nanoencapsulation of EPA/DHA with sodium caseinate-gum arabic complex and its usage in the enrichment of fruit juice. *LWT - Food Science and Technology*, *56*(2), 461–468.

Jang, K.-I., & Lee, H. G. (2008). Stability of Chitosan Nanoparticles for L -Ascorbic Acid during Heat Treatment in Aqueous Solution. *Journal of Agricultural and Food Chemistry*, *56*, 1936–1941.

Kawashima, Y., Handa, T., Kasai, A., Takenaka, H., Lin, S. Y., & Ando, Y. (1985). Novel method for the preparation of controlled-release theophylline granules coated with a polyelectrolyte complex of sodium polyphosphate–chitosan. *Journal of Pharmaceutical Sciences*, *74*(3), 264–268.

Keawchaoon, L., & Yoksan, R. (2011). Preparation, characterization and in vitro release study of carvacrol-loaded chitosan nanoparticles. *Colloids and Surfaces B: Biointerfaces*, *84*(1), 163–171.

Kim, S., Diab, R., Joubert, O., Canilho, N., & Pasc, A. (2016). Core-shell microcapsules of solid lipid nanoparticles and mesoporous silica for enhanced oral delivery of curcumin. Colloids and Surfaces. B, Biointerfaces, 140, 161–8.

Liu, Y., Xing, L., Zhang, Q., Mu, Q., & Liu, P. (2016). Thermo- and Salt-Responsive Poly (NIPAm- Co -AAc-Brij-58) Microgels : Adjustable Size , Stability under Salt Stimulus , and Rapid Protein Adsorption / Desorption. *Colloid and Polymer Science*, 294, 617–28.

Lu, F. S. H., Nielsen, N. S., Baron, C. P., Jensen, L. H. S., & Jacobsen, C. (2012). Physico-chemical properties of marine phospholipid emulsions. *JAOCS, Journal of the American Oil Chemists' Society*, *89*(11), 2011–2024.

Majeed, H., Antoniou, J., & Fang, Z. (2014). Apoptotic Effects of Eugenol-loaded Nanoemulsions in Human Colon and Liver Cancer Cell Lines. *Asian Pacific Journal of Cancer Prevention*, *15*(21), 9159–9164.

Majeed, H., Antoniou, J., Hategekimana, J., Sharif, H. R., Haider, J., Liu, F., Zhong, F. (2016). Influence of carrier oil type, particle size on in vitro lipid digestion and eugenol release in emulsion and nanoemulsions. *Food Hydrocolloids*, *52*, 415–422.

Malafaya, P. B., Silva, G. a., & Reis, R. L. (2007). Natural-origin polymers as carriers and scaffolds for biomolecules and cell delivery in tissue engineering applications. *Advanced Drug Delivery Reviews*, *59*(4-5), 207–233.

Nam, Y. S., Park, W. H., Ihm, D., & Hudson, S. M. (2010). Effect of the degree of deacetylation on the thermal decomposition of chitin and chitosan nanofibers. *Carbohydrate Polymers*, *80*(1), 291–295.

Russin, T. A., van de Voort, F. R., & Sedman, J. (2003). Novel method for rapid monitoring of lipid oxidation by FTIR spectroscopy using disposable IR cards. *Journal of the American*

Oil Chemists' Society, *80*(7), 635–641.

Sampalis, F., Bunea, R., Pelland, M. F., Kowalski, O., Duguet, N., & Dupuis, S. (2003). Evaluation of the effects of Neptune Krill Oil on the management of premenstrual syndrome and dysmenorrhea. *Alternative Medicine Review : A Journal of Clinical Therapeutic*, *8*(2), 171–9.

Schuchardt, J. P., Schneider, I., Meyer, H., Neubronner, J., von Schacky, C., & Hahn, A. (2011). Incorporation of EPA and DHA into plasma phospholipids in response to different omega-3 fatty acid formulations - a comparative bioavailability study of fish oil vs. krill oil. *Lipids in Health and Disease*, *10*(1), 145.

Shamsijazeyi, H., Miller C. A., Wong M. S., Tour, J. M., & Verduzco, R.. (2014). Polymer-Coated Nanoparticles for Enhanced Oil Recovery. *Journal of Applied polymer science* 40576, 1–13.

Shen, Z., Bhail, S., Sanguansri, L., & Augustin, M. A. (2014). Improving the oxidative stability of krill oil-in-water emulsions. *JAOCS, Journal of the American Oil Chemists' Society*, *91*(8), 1347–1354.

Terjung, N., Löffler, M., Gibis, M., Hinrichs, J., & Weiss, J. (2012). Influence of droplet size on the efficacy of oil-in-water emulsions loaded with phenolic antimicrobials. *Food & Function*, *3*(3), 290–301.

Tou, J. C., Jaczynski, J., & Chen, Y.-C. (2008). Krill for Human Consumption: Nutritional Value and Potential Health Benefits. *Nutrition Reviews*, *65*(2), 63–77.

Tur, J. A., Bibiloni, M. M., Sureda, A., & Pons, A. (2012). Dietary sources of omega 3 fatty acids: public health risks and benefits. *British Journal of Nutrition*, *107*(S2), S23–S52.

Vongsvivut, J., Heraud, P., Zhang, W., Kralovec, J. a., McNaughton, D., & Barrow, C. J. (2012). Quantitative determination of fatty acid compositions in micro-encapsulated fish-oil supplements using Fourier transform infrared (FTIR) spectroscopy. *Food Chemistry*, *135*(2), 603–9.

Voort, F. R., Ismail, A. A., Sedman, J., & Emo, G. (1994). Monitoring the oxidation of edible oils by Fourier transform infrared spectroscopy. *J. Am. Oil Chem. Soc.*, *71*(3), 243–253.

Wang, L. Y., Gu, Y. H., Zhou, Q. Z., Ma, G. H., Wan, Y. H., & Su, Z. G. (2006). Preparation and characterization of uniform-sized chitosan microspheres containing insulin by membrane emulsification and a two-step solidification process. *Colloids and Surfaces B: Biointerfaces*, *50*(2), 126–135.

Woranuch, S., & Yoksan, R. (2013). Eugenol-loaded chitosan nanoparticles: I. Thermal stability improvement of eugenol through encapsulation. *Carbohydrate Polymers*, *96*(2), 578–85.

Wu, Y., Yang, W., Wang, C., Hu, J., & Fu, S. (2005). Chitosan nanoparticles as a novel delivery system for ammonium glycyrrhizinate. *International Journal of Pharmaceutics*, *295*(1-2), 235–245.

Xu, Y., & Du, Y. (2003). Effect of molecular structure of chitosan on protein delivery properties of chitosan nanoparticles. *International Journal of Pharmaceutics*, *250*(1), 215–226.

Yang, S.-J., Lin, F.-H., Tsai, H.-M., Lin, C.-F., Chin, H.-C., Wong, J.-M., & Shieh, M.-J. (2011). Alginate-folic acid-modified chitosan nanoparticles for photodynamic detection of intestinal

neoplasms. *Biomaterials*, *32*(8), 2174–2182.

Yoksan, R., Jirawutthiwongchai, J., & Arpo, K. (2010). Encapsulation of ascorbyl palmitate in chitosan nanoparticles by oil-in-water emulsion and ionic gelation processes. *Colloids and Surfaces B: Biointerfaces*, *76*(1), 292–297.

Zainol, S., Basri, M., Basri, H. Bin, Shamsuddin, A. F., Abdul-Gani, S. S., Karjiban, R. A., & Abdul-Malek, E. (2012). Formulation Optimization of a Palm-Based Nanoemulsion System Containing Levodopa. *International Journal of Molecular Sciences*, *13*(12), 13049–13064.

Zhao, J., Wei, S., Liu, F., & Liu, D. (2014). Separation and characterization of acetone-soluble phosphatidylcholine from Antarctic krill (Euphausia superba) oil. *European Food Research and Technology*, *238*, 1023–1028.

Zhu, J., Zhuang, P., Luan, L., Sun, Q., & Cao, F. (2015). Preparation and characterization of novel nanocarriers containing krill oil for food application. *Journal of Functional Foods*, *19*, 902–912.

Zimet, P., & Livney, Y. D. (2009). Beta-lactoglobulin and its nanocomplexes with pectin as vehicles for ω-3 polyunsaturated fatty acids. *Food Hydrocolloids*, *23*(4), 1120–1126.

Highlights:

- KO loaded CSNPs were prepared using emulsion-electrostatic interaction method.
- KO loaded CSNPs were irregular in shape with average diameter of < 130 nm.
- CSNPs successfully entrap KO as evident by FTIR.
- KO loaded CSNPs prevented formation of hydroperoxides at elevated temperature.

Graphical Abstract

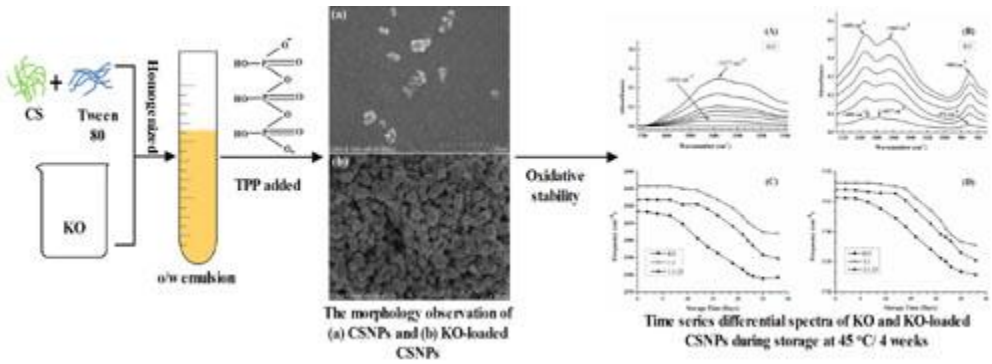

Table 1. Loading capacity (LC) and Encapsulation Efficiency (EE) of KO determined by TGA technique, intensity ration of $I_{2925}/_{890}$ determined by FTIR technique, and z-average diameter and ζ-potential value of CS and KO-loaded CSNPs.

CS : KO (w/w)	LC (%)	EE (%)	Z-average diameter [b]	ζ-potential	FTIR[a]
			(nm)	(mV)	(I_{2925}/I_{890})
1:0.00	0	0	252.0±4.9	37.7±0.0	0.91
1:0.25	8.8	58.9	229.5±3.9	35.2±0.2	1.14
1:0.50	13.3	47.1	218.6±0.3	34.3±0.9	1.42
1:0.75	18.7	41.8	217.6±2.0	31.0±0.5	1.60
1:1.00	21.8	37.0	191.3±0.2	29.5±0.2	1.81
1:1.25	24.7	33.3	182.4±1.1	26.6±0.4	1.80

LC = (weight of loaded KO/weight of sample) × 100.
EE = (weight of loaded KO/weight of KO in feed) × 100.
[a] I_{2925}/I_{890} = Indicates the intensity ration of –CH stretching peak at 2925 cm^{-1} to pyranose peak at 890 cm^{-1}.
[b] Indicated values are reported as means ± standard deviation (n = 3)

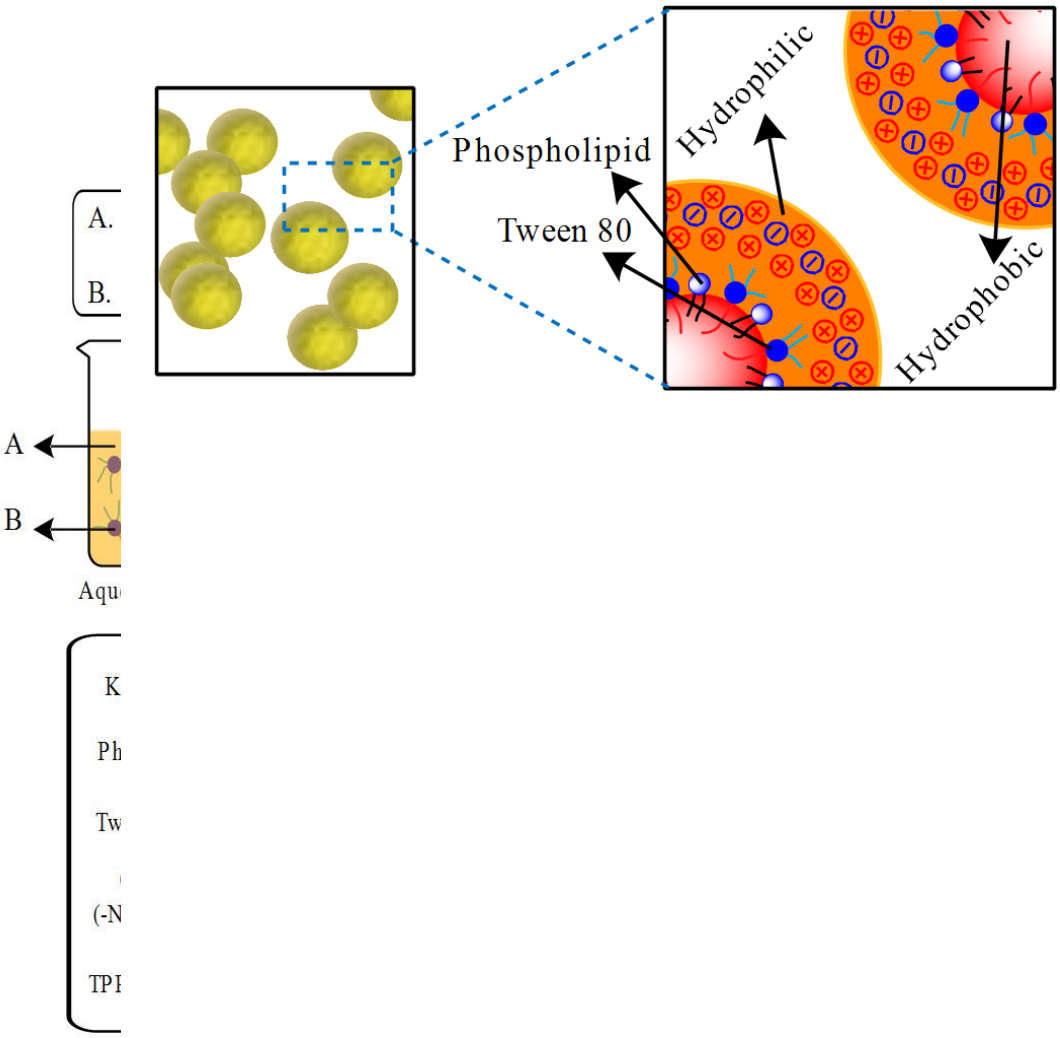

Figure 1. Schematic illustration of KO-loaded CSNPs prepared by emulsion and electrostatic interaction of CS and TPP. O/W emulsion was stabilized by synergistic effect of two amphiphiles (i.e., tween 80 and phospholipids inherent in KO) in term of emulsification. A cartoon of formed KO-loaded CSNPs (inset) indicates the entrapment of oil droplet by absorption of surfactant molecules with their hydrophilic portions (light blue and dark blue of phospholipids and tween 80 respectively) oriented toward the aqueous phase and their hydrophobic portion (black and red of phospholipids and tween 80 respectively) anchored in the oil.

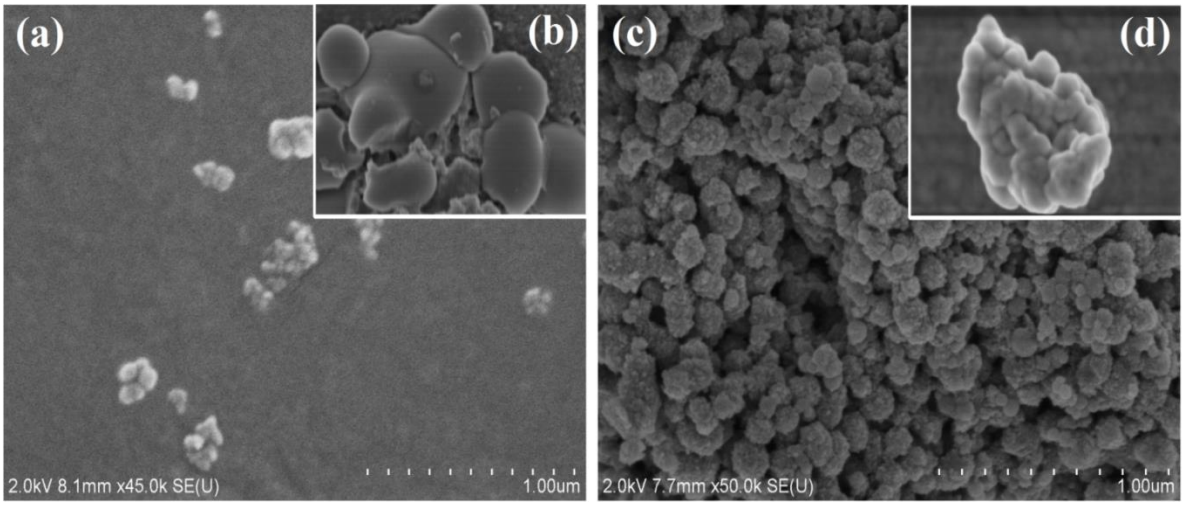

Figure 2. SEM micrographs at 2 kV of (a and b) CSNPs and (c and d) KO-loaded CSNPs prepared using an initial weight ratio of CS to KO of 1:1.00.

Figure 3. Z-average diameter, PDI and ζ-potential of CSNPs and KO-loaded CSNPs with

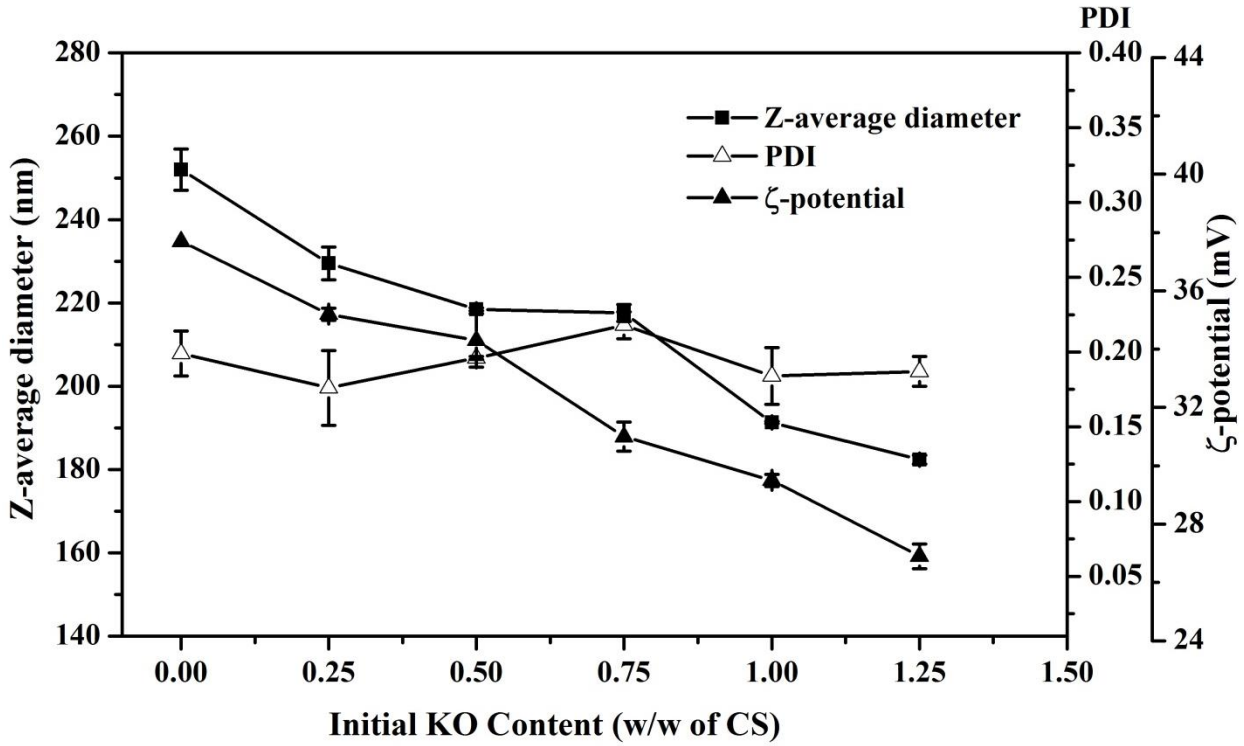

different CS to KO weight ratios. Indicated values are the means ± standard deviation (n = 3).

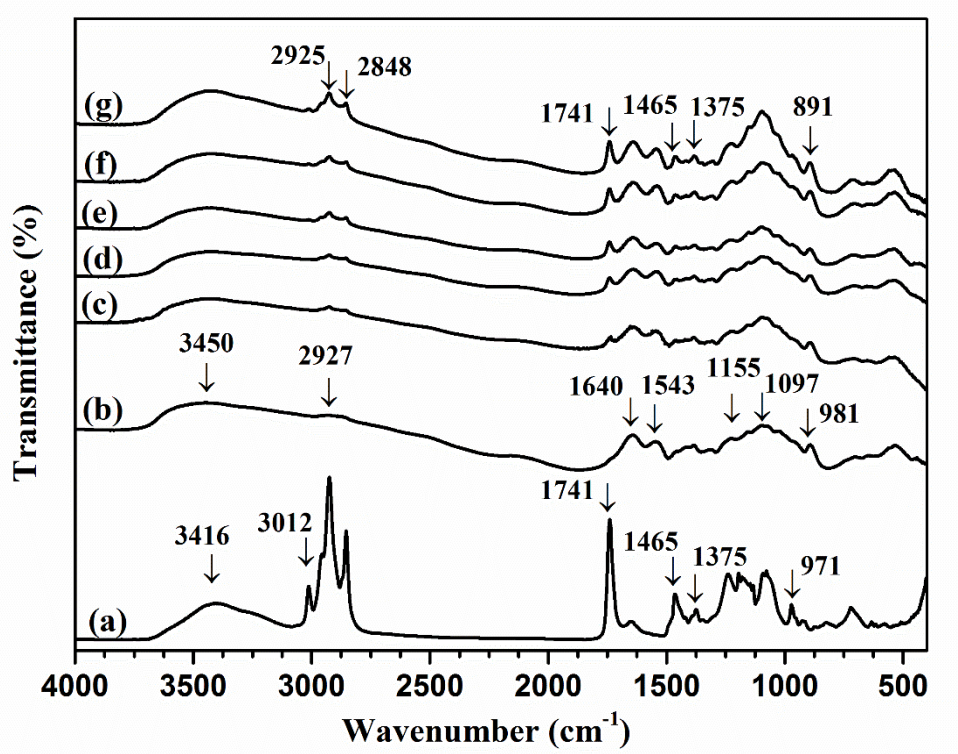

Figure 4. FTIR spectra of (a) KO, (b) CSNPs and (c)-(g) KO-loaded CSNPs prepared using different CS to KO weight ratios: (c) 1:0.25, (d) 1:0.50, (e) 1:0.75, (f) 1:1.00, (g) 1:1.25.

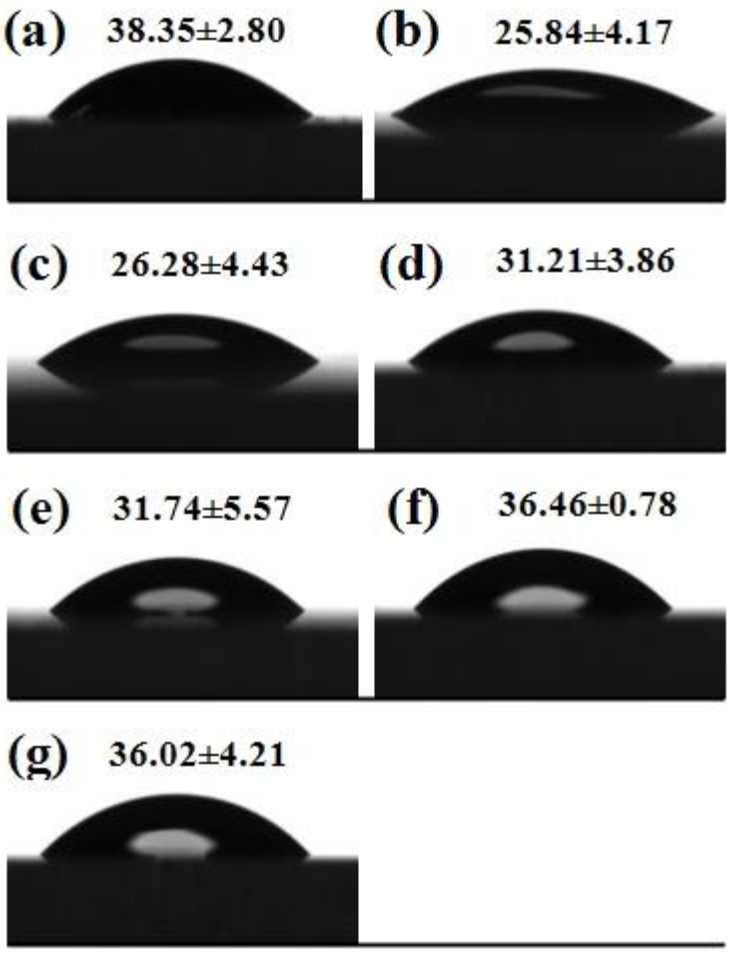

Figure 5: The surface contact angle values of (a) KO, (b) CSNPs and (c)-(g) KO-loaded CSNPs prepared using different CS to KO weight ratios: (c) 1:0.25, (d) 1:0.5, (e) 1:0.75, (f) 1:1, (g) 1:1.25

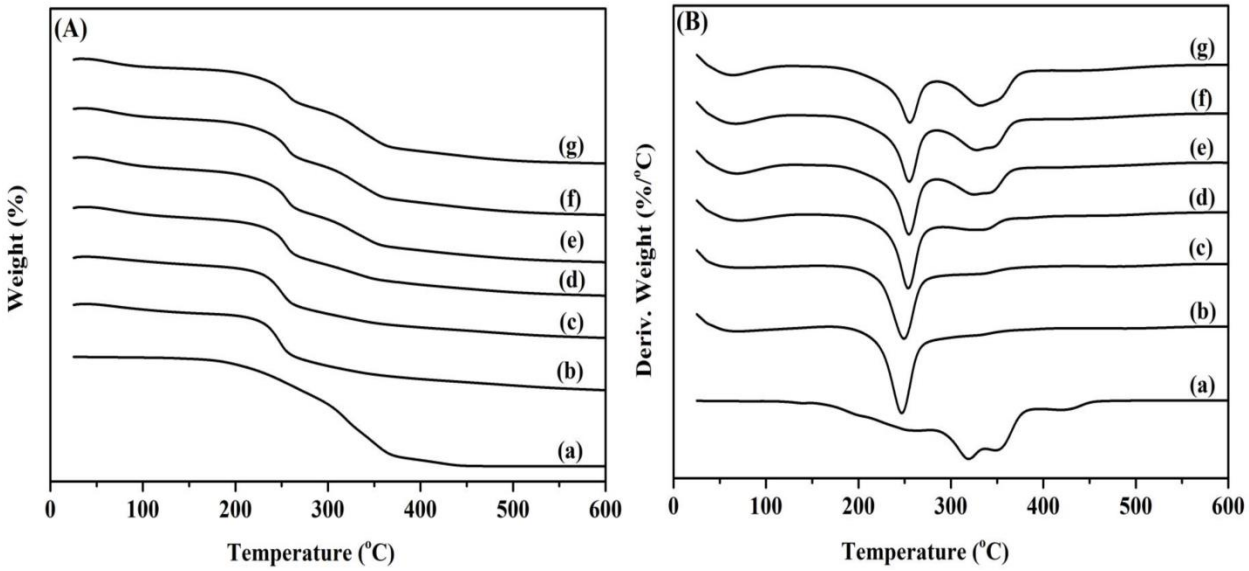

Figure 6. (A) TGA and (B) DTG thermograms of (a) KO, (b) CSNPs and (c)-(g) KO-loaded CSNPs prepared using different CS to KO weight ratios: (c) 1:0.25, (d) 1:0.50, (e) 1:0.75, (f) 1:1.00, (g) 1:1.25.

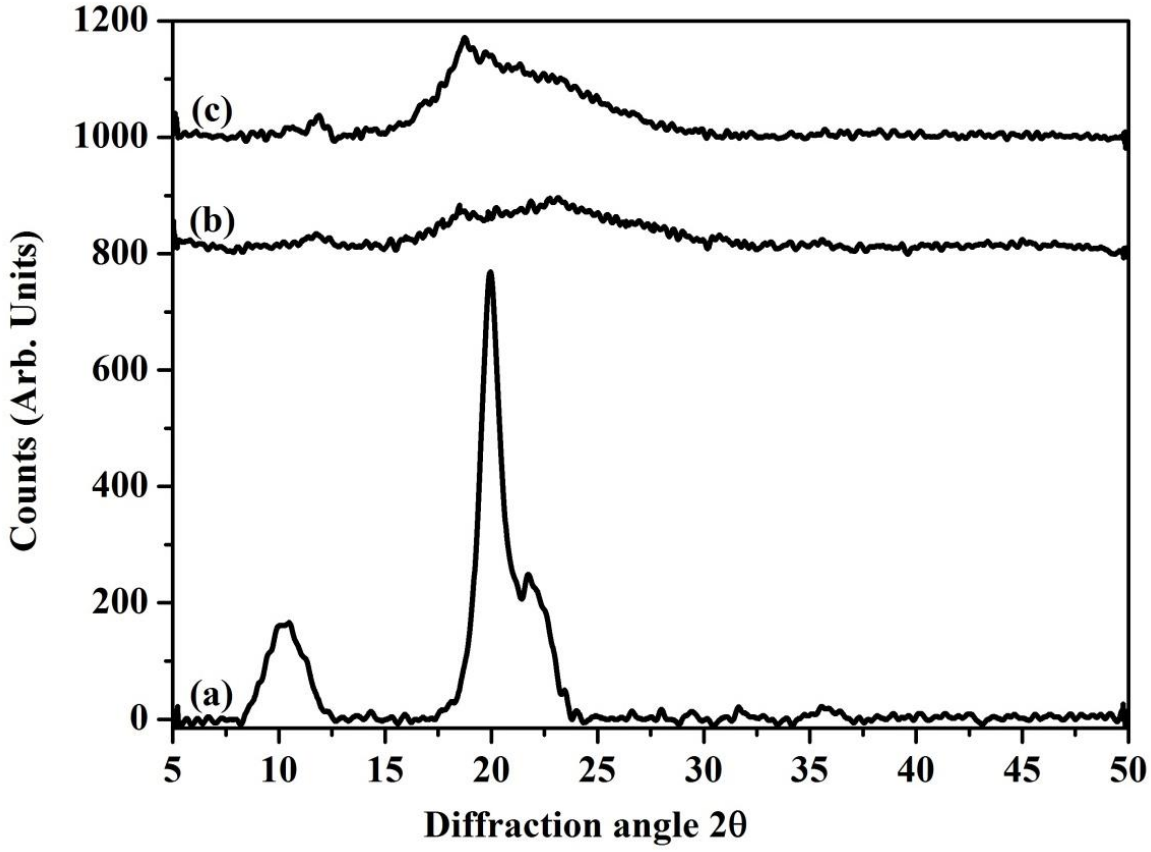

Figure 7. XRD patterns of (a) CS powder, (b) CSNPs and (c) KO-loaded CSNPs.

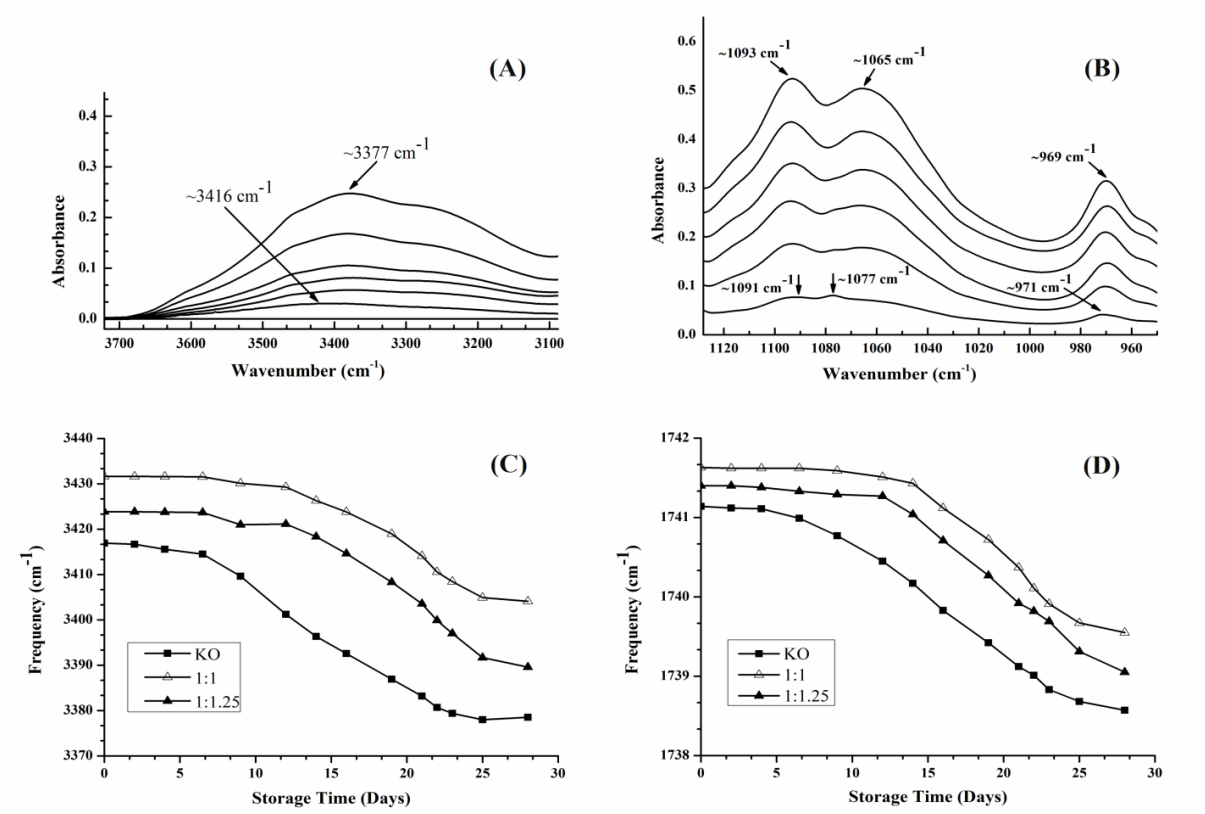

Figure 8. Time series differential spectra of KO and KO-loaded CSNPs during storage at 45 ^{o}C/ 4 weeks: (A) ROOH region of KO (~3416 to ~3377 cm^{-1}) absorptions, (B) CO region (~1091 to ~1093 cm^{-1} & ~1077 to ~1065 cm^{-1}) and *trans* region of KO (~971 to ~969 cm^{-1}) (C) Frequency values of band near ~3416 cm^{-1} (D) Frequency values of band near ~1741 cm^{-1}.